

Article

# Decaying Swirl Flow and Particle Behavior through the Hole Cleaning Device for Horizontal Drilling of Fossil Fuel

Jingyu Qu <sup>1,\*</sup>, Tie Yan <sup>1</sup>, Xiaofeng Sun <sup>1</sup>, Zijian Li <sup>2</sup> and Wei Li <sup>1</sup>

<sup>1</sup> College of Petroleum Engineering, Northeast Petroleum University, Daqing 163318, China; yant@nepu.edu.cn (T.Y.); sunxf@nepu.edu.cn (X.S.); cyyping@sina.com (W.L.)

<sup>2</sup> Department of Engineering and Applied Science, Memorial University of Newfoundland, St. John's, NF A1B3X5, Canada; zl5082@mun.ca

\* Correspondence: qjingyu@foxmail.com; Tel.: +86-459-650-3521

Received: 30 November 2018; Accepted: 19 January 2019; Published: 22 January 2019



**Abstract:** The hole cleaning device is a powerful application which can effectively slow down the deposition of cuttings during drilling. However, in this complicated swirl flow created by the device, the decay of the swirl flow and the particle behavior are not evident yet. In this paper, the decay of the swirl flow and the particle behavior in the swirl flow field are studied by the Eulerian–Eulerian two-fluid model (TFM) coupled with the kinetic theory of granular flows (KTGF), and sliding mesh (SM) technique for simulating the fluid flow. The results show that the swirl intensity decays exponentially along the flow direction under laminar flow conditions. The swirl flow has a longer acting distance at a higher rotational speed, which can effectively slow down the deposition of cutting particles. The initial swirl intensity of swirl flow induced by the blades increases significantly with the increase of blade height and the decrease of the blade angle. The tangential velocity of the cutting particles in the annulus is more significant near the central region, gradually decreases toward the wall in the radial direction, and rapidly decreases to 0 at the wall surface. The decay rate is negatively correlated with the initial swirl intensity. The results presented here may provide a useful reference for the design of the hole cleaning device.

**Keywords:** hole cleaning device; two-fluid model; decaying swirl flow; particle behavior; numerical simulation

## 1. Introduction

In recent years, with the large-scale development of complex hydrocarbon reservoirs such as low permeability, unconventional, deep water and so on, horizontal well drilling technology has become more and more widely used. The application of horizontal well technology can significantly improve oil and gas production and relieve energy stress. In the circulation of drilling fluid, cuttings particles will deposit on the lower side of the annulus and form the cuttings bed due to gravity during drilling. Insufficient cuttings transport will lead to safety problems during drilling, such as stuck pipe, high torque, and high resistance, especially in the middle-inclined section. It is reported that nearly 70% of accidents causing loss of drilling time are related to stuck pipe [1], while almost 1/3 of the drilling accidents are caused by inadequate hole cleaning [2].

So far, an extensive and in-depth experimental study has been carried out on the solid-liquid two-phase flow of cuttings particles in the annulus. Tomren et al. [3] considered that the cuttings in the middle-inclined section with an inclination angle of 35°–55° have a downward sliding tendency due to gravity. Thus, the middle-inclined section is one of the most challenging slope sections of cuttings transport. Duan et al. [4] indicated that non-Newtonian drilling fluids are more effective than

Newtonian drilling fluids in inhibiting the formation of cuttings bed. Li et al. [5] considered that the cuttings transport efficiency is the weakest for 7 mm particle diameter in the vertical well section, while in the horizontal well section the cuttings transport efficiency is the lowest for medium diameter cuttings. Ozbayoglu et al. [6] pointed out that increasing the rotational speed of the drilling pipe is more useful to improve the cuttings transport efficiency when the flow velocity of the annulus fluid is low. With the increase of annulus velocity, the effect of drilling pipe rotation gradually weakened. Han et al. [7,8] confirmed that increasing the annulus fluid velocity could enhance the effect of cuttings transport; but at the same time, the pressure drop in the annulus will increase. Allahvirdizadeh et al. [9] indicated that increasing annulus velocity is an effective method to improve the efficiency of cuttings transport; however, the increase of velocity requires an increase of pump displacement and thus an increase in cost. More dangerously, an increase in velocity will increase dynamic pressure losses in the annulus, which will cause serious accidents such as wellbore erosion and lost circulation. The flow behavior of drilling fluid and cutting particles under different drilling parameters has been widely studied [10–14]. The above researches mainly focused on the movement of cuttings under different drilling parameters and have achieved remarkable results. However, from the engineering point of view, it cannot solve the problem of cuttings deposition in the annulus during the drilling process fundamentally.

Particle transport in the pipeline has been widely researched in various scientific and engineering applications. It is possible to improve the transport capacity of particles, reduce the deposition and blockage of particles by inducing swirl flow in the pipe. Spiral wall [15], tangential inlet [16], and blades induction [17,18] have been used in many industrial fields, which have created enormous potential for engineering applications. It is an ideal hole-cleaning method to use the hole cleaning device installed on the drill pipe. It usually processes several blades on the pipe body of the drill pipe, either a straight blade or spiral blade. Moreover, it is different from the purpose of using the stabilizer; it is mainly used to induce swirl flow through the blade rotation to enhance the cuttings transport capacity in the annulus.

Since the 2010s, the application of the hole cleaning device has gradually risen and achieved a remarkable hole cleaning effect. Puymbroeck et al. [19–21] introduced a compound hole cleaning device with double helix blade small joints. Laboratory experiments and field tests show that the device has excellent cleaning ability of cuttings bed; besides, it improves the degree of hole cleaning by more than 60% and reduces the friction of drilling tools by 30%. Dave et al. [22] reported a blade-type hole cleaning device. Field experiment shows that it can effectively solve the problem of hole cleaning and poor wellbore quality. Heitmann et al. [23] reported a hole cleaning device with multi-cluster blades placed on the drill pipe. The field application shows that the drilling time can be reduced by more than 3 days with the application of this device. The wearing of casing and bit is reduced effectively. The existing literature available in this field shows its essential role. The effectiveness of this device in industrial applications is demonstrated in the literature review, but there are still some issues that need to be further explored. The above research results mainly come from macroscopic field tests and application. There is nearly no study of the decaying swirl flow and particle behavior through the hole cleaning device, the effect of changing some parameters on the hydrodynamic characteristics of the swirl flow is not completely clear. Moreover, this is also a more concerned issue in drilling engineering.

With the development of computer technology, numerical simulation technology has been widely used. It can observe many flow details that are difficult to obtain in experiments. It has been successfully applied to the study of particle transport in swirling flow [24–26]. In this paper, a computational fluid dynamics (CFD) technique was used to establish a three-dimensional numerical model of the flow based on the experimental model of Han et al. (2010). Coupling with the kinetic theory of granular flows (KTGF) using the Eulerian–Eulerian two-fluid model (TFM) approach, the blade rotation is achieved using the sliding mesh (SM) technique. The effects of different parameters of the hole cleaning device on the decaying swirl flow induced by non-Newtonian drilling fluid, the particle behavior and settlement of cutting particles have been studied.

## 2. Computational Methodology

Since in the viewpoint of Eulerian–Eulerian both liquid and solid phases are considered as a continuous phase, then useful information can be obtained to analyze the results as well as the lower computational cost than the Eulerian–Lagrangian approach. Consequently, in this paper, TFM is utilized to solve liquid–solid two-phase flow. The interaction between the liquid and solid is explained by KTGF model. The simulation makes the following simplification: (1) the particles are all standard spherical particles; (2) the particle size of all particles remained consistent; (3) heat transfer between two phases is not involved.

### 2.1. Conservation Equations

The continuity equation of drilling fluid and cuttings are expressed as:

$$\frac{\partial}{\partial t}(\alpha_l \rho_l) + \nabla \cdot (\alpha_l \rho_l \mathbf{u}_l) = 0 \quad (1)$$

$$\frac{\partial}{\partial t}(\alpha_s \rho_s) + \nabla \cdot (\alpha_s \rho_s \mathbf{u}_s) = 0 \quad (2)$$

$$\alpha_l + \alpha_s = 1 \quad (3)$$

where,  $l$  and  $s$  are the representative indexes for drilling fluid and cuttings, respectively;  $\alpha$  is the volume fraction;  $\mathbf{u}$  is the velocity vector;  $\rho$  is the density. Each computational cell is shared by the interpenetrating phases so that the sum of their volume fractions is unity.

The momentum equation of drilling fluid is expressed as:

$$\frac{\partial}{\partial t}(\alpha_l \rho_l \mathbf{u}_l) + \nabla \cdot (\alpha_l \rho_l \mathbf{u}_l \mathbf{u}_l) = \alpha_l \nabla \cdot \boldsymbol{\tau}_l + \alpha_l \rho_l \mathbf{g} - \alpha_l \nabla p - \beta(\mathbf{u}_l - \mathbf{u}_s) \quad (4)$$

Moreover, for the cuttings,

$$\frac{\partial}{\partial t}(\alpha_s \rho_s \mathbf{u}_s) + \nabla \cdot (\alpha_s \rho_s \mathbf{u}_s \mathbf{u}_s) = -\alpha_s \nabla p - \nabla p_s + \alpha_s \nabla \cdot \boldsymbol{\tau}_s + \alpha_s \rho_s \mathbf{g} + \beta(\mathbf{u}_l - \mathbf{u}_s) \quad (5)$$

where  $\mathbf{g}$  is the acceleration due to gravity;  $\boldsymbol{\tau}$  is the stress tensor;  $p$  is the pressure;  $p_s$  is the solids pressure;  $\beta$  is the interface momentum transfer coefficient.

The drilling fluid is a non-Newtonian fluid (power-law fluid), which is a 0.4% carboxymethylcellulose (CMC) solution. The constitutive equation of power-law fluid is expressed as:

$$\boldsymbol{\tau}_l = \eta(\dot{\boldsymbol{\gamma}}) \cdot \dot{\boldsymbol{\gamma}} \quad (6)$$

$$\dot{\boldsymbol{\gamma}} = \left( \frac{\partial u_{lj}}{\partial x_i} + \frac{\partial u_{li}}{\partial x_j} \right) \quad (7)$$

where  $\dot{\boldsymbol{\gamma}}$  is the rate of deformation tensor;  $\eta(\dot{\boldsymbol{\gamma}})$  is the apparent viscosity, which is a function of the shear rate expressed as:

$$\eta(\dot{\boldsymbol{\gamma}}) = \kappa \left( \frac{1}{2} \dot{\boldsymbol{\gamma}} : \dot{\boldsymbol{\gamma}} \right)^{\frac{n-1}{2}} \quad (8)$$

where  $\kappa$  and  $n$  are the fluid consistency index and the flow behavior index. The drilling fluid is a Newtonian fluid when  $n = 1$ , while it is shear thinning fluid when  $n < 1$ , or shear thickening fluid when  $n > 1$ .

The shear stress of cuttings is expressed as:

$$\boldsymbol{\tau}_s = \mu_s \left\{ \left[ \nabla \mathbf{u}_s + (\nabla \mathbf{u}_s)^T \right] - \frac{2}{3} (\nabla \cdot \mathbf{u}_s) \mathbf{I} \right\} + \xi_s \nabla \cdot \mathbf{u}_s \mathbf{I} \quad (9)$$

where  $\mathbf{I}$  is a unit vector;  $\zeta_s$  and  $\mu_s$  are the bulk solids viscosity and shear viscosity of cuttings. The granular temperature transport equation (algebraic formulation) is expressed as follows:

$$0 = (-p_s \mathbf{I} + \boldsymbol{\tau}_s) : \nabla \mathbf{u}_s - \gamma_{\Theta_s} + \varphi_{ls} \quad (10)$$

where  $\Theta_s$  is the granular temperature;  $(-p_s \mathbf{I} + \boldsymbol{\tau}_s) : \nabla \mathbf{u}_s$  is the generation of energy by the solid stress tensor;  $\gamma_{\Theta_s}$  is the collisional dissipation of energy;  $\varphi_{ls}$  is the energy exchange between the fluid or solid phase and the solid phase.

Solids pressure  $p_s$  is defined as:

$$p_s = \alpha_s \rho_s \Theta_s + 2\rho_s(1+e)\alpha_s^2 g_0 \Theta_s \quad (11)$$

While  $e$  is the restitution coefficient of particle collisions;  $g_0$  is the radial distribution function which is modeled as below:

$$g_0 = \left[ 1 - \left( \frac{\alpha_s}{\alpha_{s\max}} \right)^{\frac{1}{3}} \right]^{-1} \quad (12)$$

The solid shear viscosity can be represented as the following equation:

$$\mu_s = \frac{4}{5} \alpha_s \rho_s d_s g_0 (1+e) \sqrt{\frac{\Theta_s}{\pi}} + \frac{10\rho_s d_s \sqrt{\pi\Theta_s}}{96(1+e)\alpha_s g_0} \left[ 1 + \frac{4}{5} g_0 \alpha_s (1+e) \right]^2 \quad (13)$$

The solids bulk viscosity accounts for the resistance of the granular particles to compression and expansion:

$$\zeta_s = \frac{4}{3} \alpha_s \rho_s d_s g_0 (1+e) \sqrt{\frac{\Theta_s}{\pi}} \quad (14)$$

For liquid–solid two-phase systems, the drag force between particles and fluid is the most influential force in the interaction between the phases. At present, the most common drag models include the Syamlal–O’Brien model [27], the Wen and Yu model [28], and the Gidaspow model [29]. Among them, the Gidaspow model is the most commonly used, which has a good prediction accuracy [30,31]. The Gidaspow model is a combination of the Ergun model [32] and the Wen and Yu model. For liquid concentrations greater than 0.8, momentum exchange coefficient between liquid and solid phase  $\beta$  is determined by the Wen and Yu model; whereas for values less than or equal to 0.8, exchange coefficient  $\beta$  is determined by the Ergun model. However, the drag function of the Gidaspow model is discontinuous with the change of the solid volume fraction, which is contrary to the physical law. The drag force is a continuous function of the solid phase volume fraction and Reynolds number. Therefore, an improved Gidaspow model is proposed to correct the discontinuity of the drag function [33]. In this model, the momentum exchange coefficient between liquid and solid is as follows:

$$\beta_{Huilin-Gidaspow} = \varphi \beta_{Ergun} + (1 - \varphi) \beta_{Wen\&Yu} \quad (15)$$

$$\varphi = \frac{\arctan[262.5(\alpha_s - 0.2)]}{\pi} + 0.5 \quad (16)$$

$$\beta_{Wen\&Yu} = \frac{3}{4} C_D \frac{\alpha_s \alpha_l \rho_l |\mathbf{u}_s - \mathbf{u}_l|}{d_s} \alpha_l^{-2.65} \quad (17)$$

$$\beta_{Ergun} = 150 \frac{\alpha_s (1 - \alpha_l) \mu_l}{\alpha_l d_s^2} + 1.75 \frac{\rho_l \alpha_s |\mathbf{u}_s - \mathbf{u}_l|}{d_s} \quad (18)$$

where the drag coefficient  $C_D$ , is:

$$C_D = \frac{24}{Re_s} (1 + 0.15 Re_s^{0.687}), Re_s \leq 1000 \quad (19)$$

$$C_D = 0.44, Re_s > 1000 \quad (20)$$

$Re_s$  is the particle Reynolds number is defined as:

$$Re_s = \frac{\rho_l d_s |\mathbf{u}_s - \mathbf{u}_l|}{\mu_l} \quad (21)$$

## 2.2. Model Geometry and Boundary Conditions

In this work, the geometric model is consistent with the experimental model of Han et al. (2010). The annulus is composed of the inner surface of a drill pipe and the outer surface of a casing. The hole-cleaning device is simulated by the spiral blades placed on the drill pipe. According to the formula proposed by Shook and Roco [34] in the single-phase case, the length of the inlet section of laminar flow is calculated to ensure that the fluid is in the complete development stage before entering the area of the blade.

$$\frac{L_e}{D} = 0.062 Re_D \quad (22)$$

$$Re_D = \frac{\rho U_{in} D_h}{\mu} \quad (23)$$

where  $Re_D$  is the Reynold number,  $D_h$  is the hydraulic diameter,  $U_{in}$  is the axial velocity. Based on the above formula, pipe diameter  $D$  is replaced by the hydraulic diameter  $D_h$ , and the length of the inlet section is calculated. The hole cleaning device is placed on the wall of the drill pipe at 0.4 m from the inlet; the overall length of the device is 0.1 m. The height of blade ranges from  $h/D_h = 0.1$  to 0.4 while blades with angles of  $\alpha = 0^\circ, 10^\circ, 20^\circ$ , and  $30^\circ$  are used for the study. The primary input parameters adopted in the model are shown in Table 1.

**Table 1.** Summarized input parameters in the simulation.

Properties	Values	Units
Drill string length ( $L$ )	1.8	m
Angle of inclination ( $\theta$ )	45	deg
Pipe diameter ( $D_0$ )	30	mm
Hole diameter ( $D_1$ )	44	mm
Eccentricity ( $e$ )	0	-
Drill pipe rotational speed ( $\omega$ )	100, 200, 300, 400	rpm
Fluid inlet velocity ( $U_{in}$ )	0.49	m/s
Fluid density ( $\rho_l$ )	998.5	kg/m <sup>3</sup>
Power law exponent ( $n$ )	0.75	-
Consistency factor ( $k$ )	0.048	Pa·s <sup>n</sup>
Particle density ( $\rho_s$ )	2550	kg/m <sup>3</sup>
Particle diameter ( $d_s$ )	2	mm
Injected particle volume fraction ( $C_v$ )	4	%
Blade angle ( $\alpha$ )	0, 10, 20, 30	deg
Blade height ( $h/D_h$ )	0.1, 0.2, 0.3, 0.4	-

The two-phase flow system of drilling fluid and uniformly dispersed cuttings particles enter into the annular space from the inlet and exit from the outlet. Velocity inlet and pressure outlet boundary conditions are used for entrance and exit, the gauge pressure at the outlet is zero. The no-slip boundary condition is used for the wall. The sliding mesh technique is used to realize the rotation of the blade domain. The momentum and mass exchange between static and rotating domains is accomplished by the interface.

## 2.3. Discretization and Numerical Solution

Appropriate mesh generators and high precision mesh quality are essential prerequisites for CFD computation. To improve the accuracy of the calculation, to speed up the calculation and to

convergence speed, as shown in Figure 1, the flow field in this work is divided into hexahedron structure mesh, while the mesh near the hole cleaning device is refined and processed, the first layer mesh thickness is 0.5 mm in the simulation.

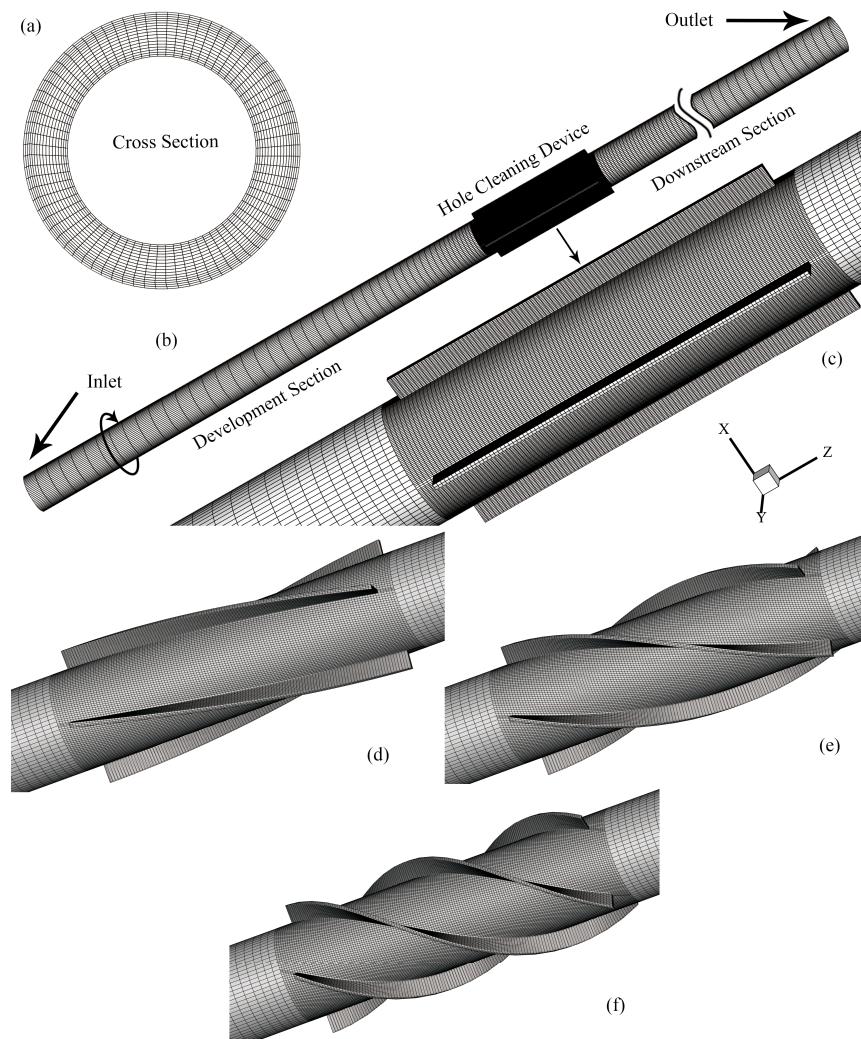


**Figure 1.** 3D view of the computational domain including hole cleaning device: (a) cross-sectional view; (b) entire grid system; (c)  $\alpha = 0^\circ$ ; (d)  $\alpha = 10^\circ$ ; (e)  $\alpha = 20^\circ$ ; (f)  $\alpha = 30^\circ$ .

To verify the independence of the grid models, 512,055, 688,543, and 872,045 mesh elements are used to simulate the flow field. The results in Table 2 show that the relative error regarding both the pressure drop and mean tangential velocity is less than 4% when using grid numbers of 688,543, and 872,045. Considering the required precision and the cost of grid computing, finally nearly 688,000 grid is chosen in the simulation.

**Table 2.** Grid independence tests.

Grid Model	Pressure Drop (Pa/m)	Relative Error	Mean Tangential Velocity at Sampling Surface (m/s)	Relative Error
512,055	1416.7	-	0.0192	-
688,543	1368.8	3.50%	0.0185	3.78%
872,045	1360.1	0.64%	0.0183	1.09%

Three-dimensional and transient simulations have been carried out. After the discretization of governing equations by the finite volume method, the phase-coupled SIMPLE algorithm is applied

to the pressure–velocity coupling. Gradients are estimated using a least squares cell-based method. The momentum and the volume fraction interpolation are discretized using the QUICK routine due to its better adaptation to hexahedral mesh. Time integrations are performed with a second-order implicit scheme [35]. The relative error between two successive iterations is specified by using a convergence criterion for the continuity equation, velocity and volume fraction of  $10^{-5}$  for each scaled residual component. A time step of 0.001 s with 20 iterations per time step is chosen. All of the simulations in this work are performed on the Core i7 processor with 8 cores and a total memory size of 16 GB RAM.

### 3. Results and Discussion

#### 3.1. Validation of the Computational Model

The swirl number  $S_n$  is usually used to characterize the magnitude of swirl intensity and the effect of swirl on particle deposition. Swirl number  $S_n$  is a dimensionless parameter, first proposed by Chigier and Beer [36]. It is defined as the ratio of the axial flux of angular momentum to the axial flux of axial momentum on the desired surface, widely used in the literature:

$$S_n = \frac{\int_{R_0}^{R_1} u\omega r^2 dr}{R_1 \int_{R_0}^{R_1} u^2 r dr} \quad (24)$$

$R_1$  and  $R_0$  represent the radius of the casing and drill pipe. It is shown by many scholars that the swirl number  $S_n$  induced by swirling flow in the annulus agrees with the exponential distribution along the axial direction due to the friction loss of the pipe wall and the viscous shear effect of the fluid. The decay of the swirl flow can be evaluated by the decay rate  $\beta$ , which is the primary parameter to study the swirl flow. The decay law of swirl intensity can be expressed by the following formula:

$$S_n = S_0 \exp\left(-\beta \frac{L}{D_h}\right) \quad (25)$$

In the equation,  $L$  is the distance behind the blade;  $\beta$  is the magnitude of the decay rate;  $S_0$  is the initial swirl intensity.

To verify the rationality of the selected numerical model, a numerical simulation of decaying swirl flow in single-phase flow and solid–liquid two-phase flow in the annulus is carried out. Then, the comparison between the experimental data and the predicted results is given in Figure 2. The experimental data agree well with the simulation results, which prove the reliability and accuracy of the current numerical model.

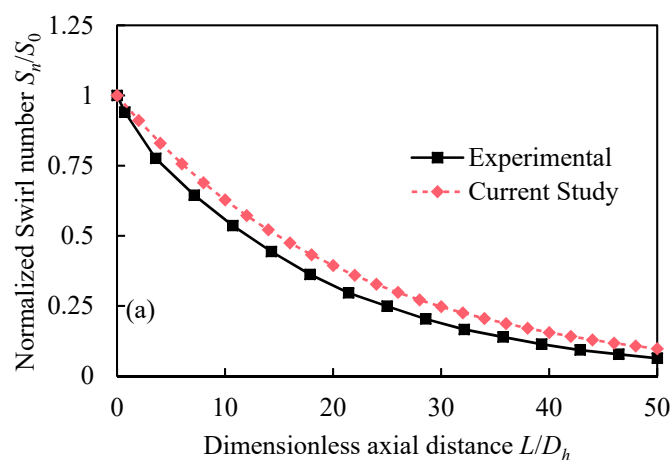


Figure 2. Cont.

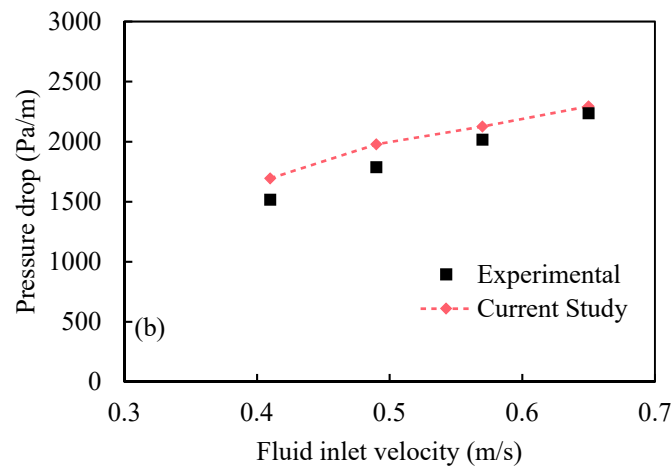


Figure 2. Comparison of simulation: (a) Fokeer et al.’s experiments [24]; (b) Han et al.’s experiments [8].

### 3.2. Effect of the Rotational Speed of Hole Cleaning Performance

The decay of swirl intensity  $S_n$  induced by single-phase drilling fluid at a different blade rotational speed (100, 200, 300, and 400 rpm) along the axial direction is shown in Figure 3, with a blade angle of  $0^\circ$  and a blade height of  $h = 0.4 D_h$ . At different rotational speed, the swirl number  $S_n$  decay exponentially along the axial direction, which is consistent with the study from articles [24–26].

The higher the rotational speed of the blade, the greater the initial swirl strength  $S_0$  of the swirl flow. Also, the contribution of increasing rotational speed to the initial swirl intensity  $S_0$  is more evident in the low rotational speed. Under the conditions of 200 rpm, 300 rpm, and 400 rpm, the initial swirl intensity  $S_0$  increases by 96.5%, 44.0%, and 26.8% respectively with the rise of 100 rpm speed. At the same time, the fitted curve of different rotational speed agrees with an exponential curve.

The decay rate  $\beta$  decreases slightly with the increase of rotational speed, while the decay of swirling flow at high rotational speed is slower than that at low speed. Therefore, it is indicated that the fluid with a higher swirl strength is more resistant to wall friction and viscous fluid loss.

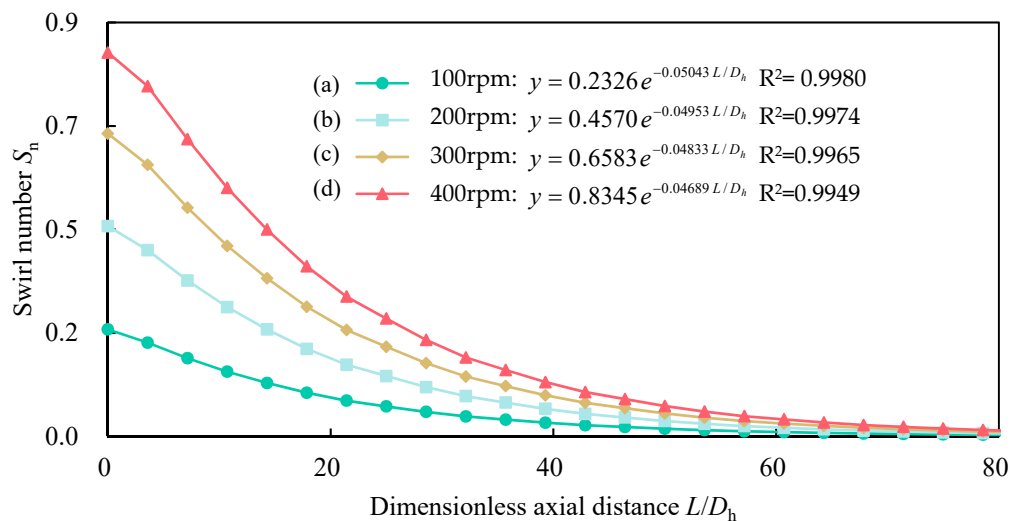
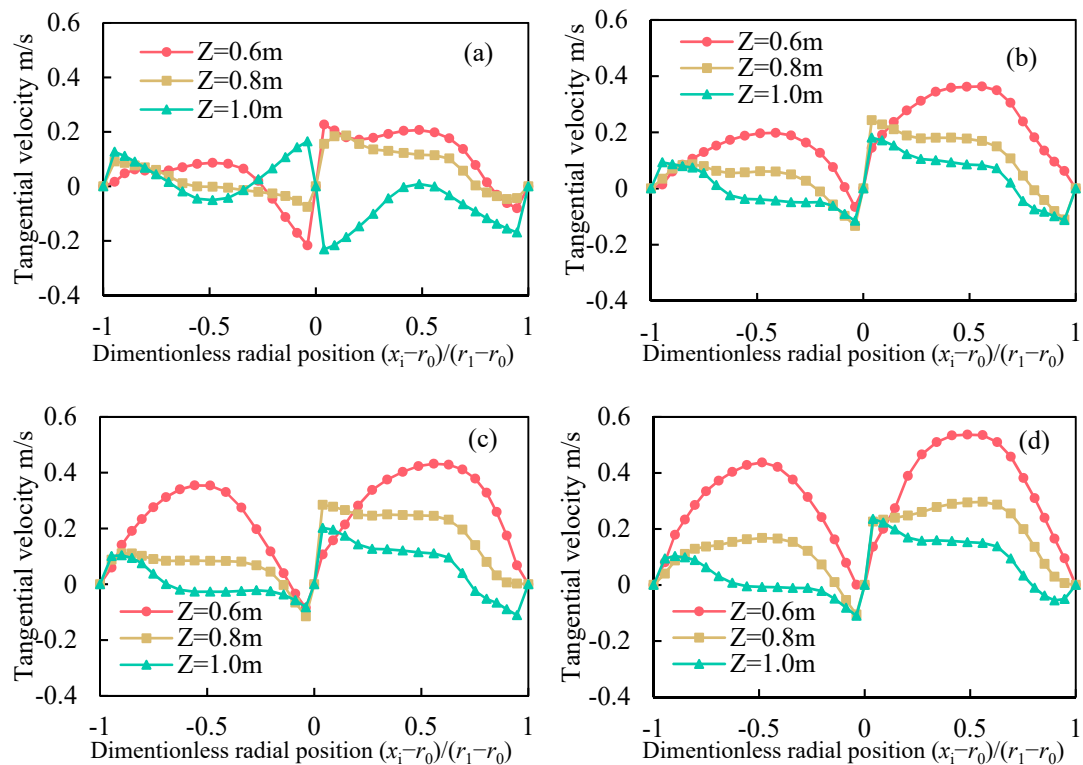


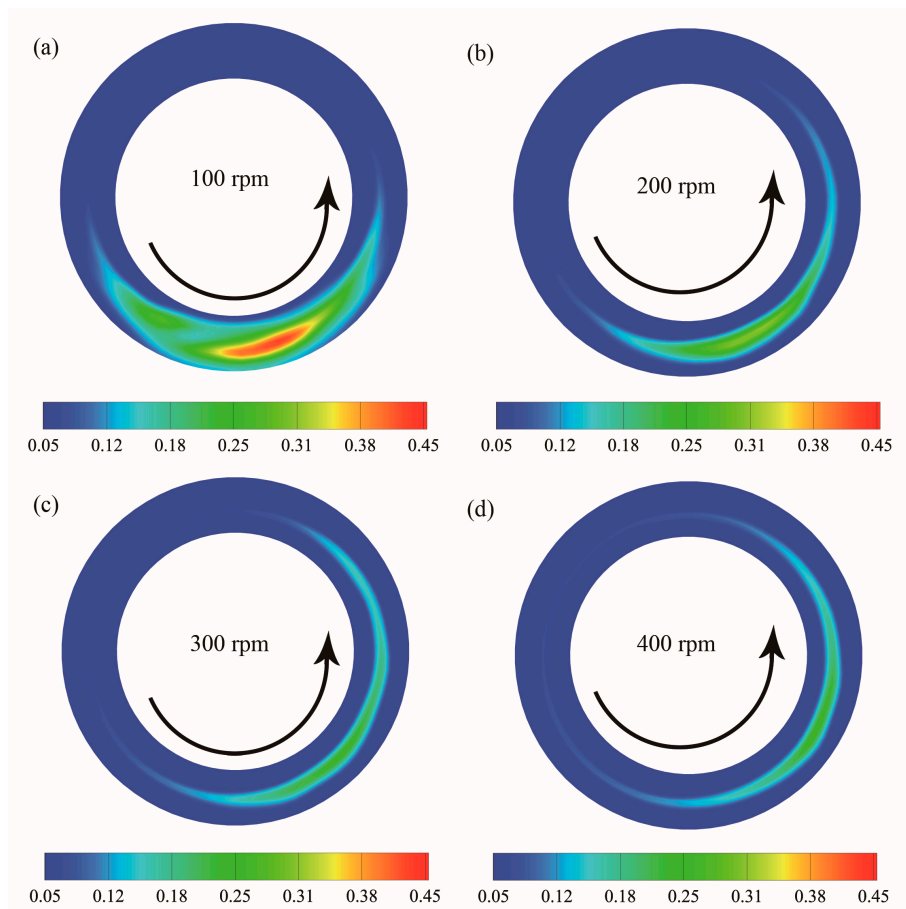
Figure 3. The effect of rotational speed on the swirl number: (a) 100 rpm; (b) 200 rpm; (c) 300 rpm; (d) 400 rpm.

Figure 4 shows the tangential velocity distribution of cuttings particles with the blade angle of  $0^\circ$  and the blade height of  $h = 0.4D_h$  at the different cross sections ( $z = 0.6$  m,  $0.8$  m, and  $1.0$  m). At higher rotational speed (Figure 4b–d), the tangential velocity of cuttings on different sections decreases with the increase of axial displacement. Besides, a more considerable tangential velocity is observed in the core region far from the wall. The maximum tangential velocity can exceed  $0.54$  m/s at  $200$  rpm, which gradually decrease toward the wall in the radial direction, and rapidly drops to  $0$  on the wall surface. Since the high swirl can transfer higher momentum, the tangential velocity of the swirl increases with the increase of the rotational speed in the same cross-section.



**Figure 4.** The tangential velocity of particles at different cross section: (a) 100 rpm; (b) 200 rpm; (c) 300 rpm; (d) 400 rpm.

Figure 5 shows the particle concentration contours at an axial position of  $z = 1.0$  m at four different rotational speed (100, 200, 300, and 400 rpm). The initial swirl intensity of the swirl flow induced by the blade is great at a high rotational speed and continues to decay along the flow direction. At the same cross-sectional position, the swirl intensity effect of the fluid at a high rotational speed (Figure 5b–d) is still active, and more of the cuttings particles will be suspended in the annulus. However, at a low rotational speed (Figure 5a), the swirl effect of the fluid is weak, and the deposition of cuttings in the annulus is more pronounced due to gravity.



**Figure 5.** Contours of the cuttings volume fraction of different rotational speed: (a) 100 rpm; (b) 200 rpm; (c) 300 rpm; (d) 400 rpm.

### 3.3. Effect of Blade Height and Blade Angle on Hole Cleaning Performance

The blade height  $h$  and helical angle  $\alpha$  are two important structural parameters of the blade. Figures 6 and 7 show the columnar distribution of the initial swirl intensity  $S_0$  and the fitted decay rate  $\beta$  at different blade height  $h$  and helical angle  $\alpha$  under single-phase conditions.

It can be seen in Figure 6 that the initial swirl intensity  $S_0$  decreases with the increase of blade angle while the trend becomes more evident with the rise of blade height. When the blade height is  $h = 0.1D_h$ , the change of initial swirl intensity  $S_0$  caused by four blade angles is not more than 43.0%. However, when blade height is  $h = 0.4D_h$ , it has reached 298.5%. It is indicated that the initial swirl intensity is very sensitive to the blade angle at high blade height. When the blade angle is  $\alpha = 30^\circ$ , the increase of blade height  $h$  has little effect on the initial swirl intensity  $S_0$ . However, at a smaller blade angle ( $\alpha = 0^\circ, 10^\circ, \text{ and } 20^\circ$ ), the increase of blade height will increase the initial swirl intensity. For example, at  $\alpha = 0^\circ, h = 0.4D_h$ , the initial swirl intensity  $S_0$  of swirl flow induced by the blade can reach  $S_0 = 0.66$ . However, this tendency decreases rapidly with the increase of the blade angle. It is indicated that the initial swirl intensity is very sensitive to the blade height at a low blade angle.

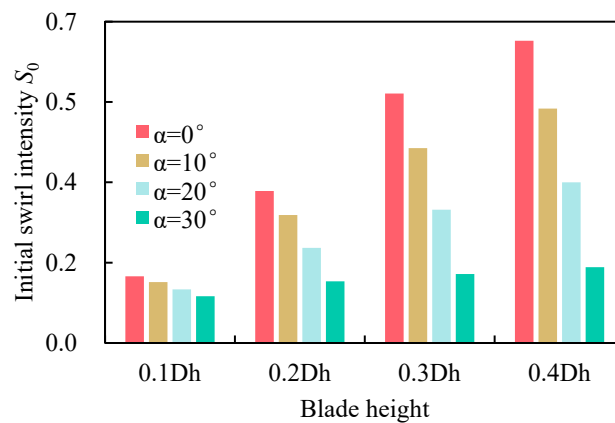


Figure 6. Effect of blade height and blade angle on initial swirl intensity.

Visible from the histogram in Figure 7 shows that the decay rate  $\beta$  of swirl flow induced by the blade is almost unchanged at low blade height. Once the blade height increases, the decay rate will increase significantly with the rise of the blade angle. The higher the blade height is, the stronger this trend is. For example, at  $h = 0.4D_h$ , the difference between  $\alpha = 0^\circ$  and  $\alpha = 30^\circ$  can reach 12.7%. It indicates that the initial swirl intensity  $S_0$  has a negative correlation with decay rate  $\beta$ . When the blade height is small ( $h = 0.1D_h$ ), the swirl intensity of the swirl flow induced by the blade is lower and will decrease rapidly. When the blade height increases ( $h = 0.3D_h$  and  $0.4D_h$ ), the effect of the change in the blade angle on the initial swirl intensity and the rate of decay is significantly improved.

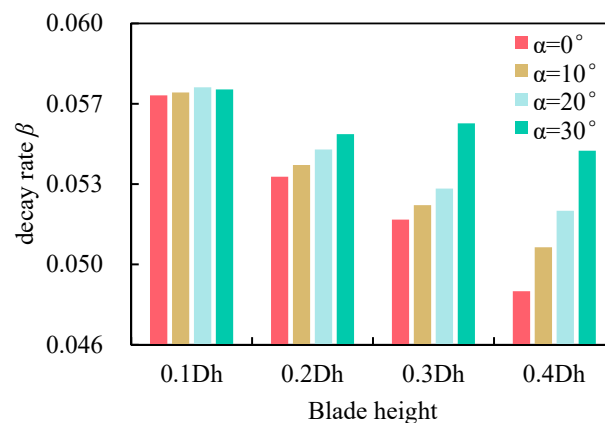
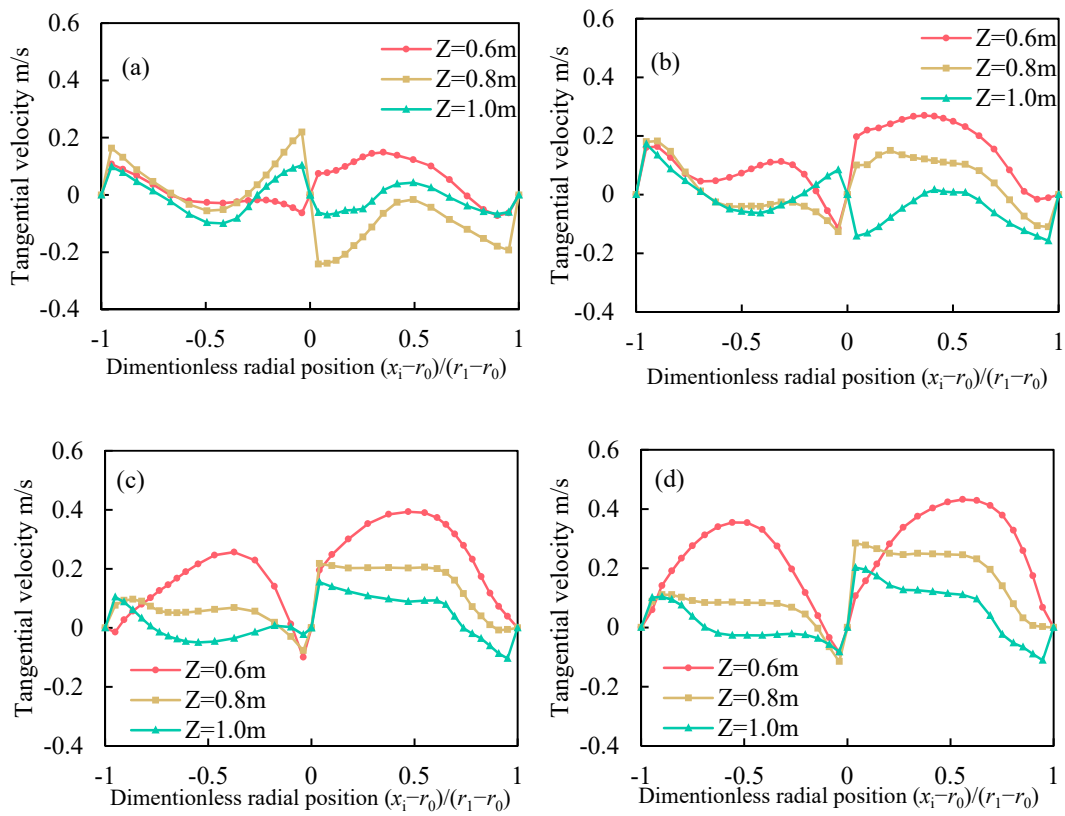


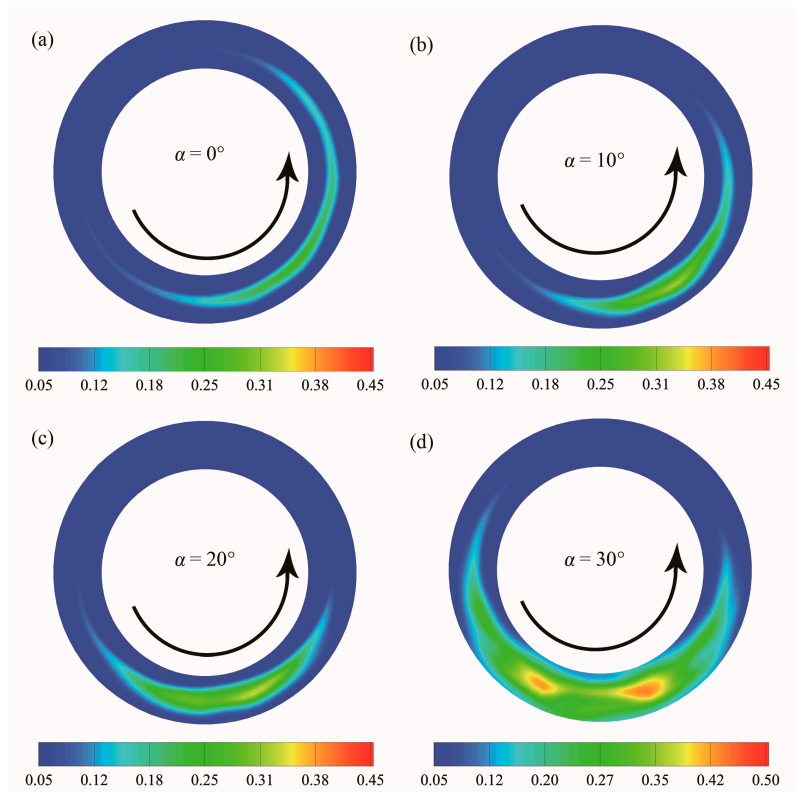
Figure 7. Effect of blade height and blade angle on the decay rate.

Figure 8 shows the tangential velocity distribution curves of cutting particles at four blade height at different cross-section positions ( $z = 0.6 \text{ m}$ ,  $0.8 \text{ m}$ , and  $1.0 \text{ m}$ ) with rotational speed at 300 rpm and blade angle  $\alpha = 0^\circ$ . It can be seen from the diagram that as the increase of the blade height (Figure 8b–d), the tangential velocity of the particles increases due to the circumferential force exerted by the drilling fluid. The tangential speed can reach up to 0.56 m/s. At the same blade height, with the increase of axial displacement, the tangential velocity of cuttings to decrease rapidly.

Figure 9 shows the particle concentration contours at an axial position of  $z = 1.0 \text{ m}$  at four different blade angles. Because the initial swirl intensity decreases rapidly with the increase of blade angle at a higher blade height, the larger the blade angle is, the weaker the swirling effect of the drilling fluid is at the cross-section of  $z = 1.0 \text{ m}$ . It indicates that the cuttings are more likely to deposit at the bottom of the annulus at a higher blade angle, like Figure 9d. On the contrary, the smaller the blade angle is (such as Figure 9a), the stronger the swirling effect of drilling fluid and there will be more particles suspended in the annulus, it becomes more difficult for cuttings to deposit at the bottom of the annulus.



**Figure 8.** The tangential velocity of particles at different cross section: (a)  $h = 0.1D_h$ ; (b)  $h = 0.2D_h$ ; (c)  $h = 0.3D_h$ ; (d)  $h = 0.4D_h$ .



**Figure 9.** Contours of the cuttings volume fraction of different blade angle: (a)  $\alpha = 0^\circ$ ; (b)  $\alpha = 10^\circ$ ; (c)  $\alpha = 20^\circ$ ; (d)  $\alpha = 30^\circ$ .

#### 4. Conclusions

In this paper, a TFM model coupled with KTGF is used to study the effect of various parameters on the decay swirl flow and the particle behavior through the hole cleaning device. The following conclusions can be drawn from the obtained modeling results:

- (1) Swirl number  $S_n$  decays exponentially along the flow direction. Additionally, the increase of rotational speed can significantly increase the initial swirl intensity  $S_0$  of the swirl flow induced by the blade.
- (2) Increasing the height of the blade  $h$  and reducing the blade angle  $\alpha$  can lead to an increase in the initial swirl intensity  $S_0$  of the swirl flow and cause a lower decay rate  $\beta$ . The decay rate  $\beta$  is negatively correlated with the initial swirl intensity  $S_0$ .
- (3) The tangential velocity of the cutting particles in the annulus is more significant near the central region, gradually decreasing in the direction of the radial wall.
- (4) To minimize the problem of cuttings particles deposition in the annulus, the hole cleaning device is needed to increase the greater initial swirl intensity  $S_0$  and lower swirl decay rate  $\beta$ . On the whole, the work provides strong design input to the hole cleaning device.

**Author Contributions:** Conceptualization, J.Q.; Data curation, Z.L.; Methodology, J.Q. and X.S.; Software, J.Q. and X.S.; Supervision, T.Y.; Visualization, W.L.; Writing—original draft, J.Q.; Writing—review and editing, T.Y. and W.L.

**Funding:** This research was funded by the National Natural Science Foundation of China (Grant No. 51674087) and National Science and Technology Major Project of the Ministry of Science and Technology of China (Project No. 2017ZX05009-003).

**Acknowledgments:** The authors would like to express sincere appreciation to the editor and the anonymous reviewers for their valuable comments and suggestions for improving the presentation of the manuscript.

**Conflicts of Interest:** The authors declare no conflict of interest.

#### References

1. Massie, G.W.; Castlesmith, J.; Lee, J.W.; Ramsey, M.S. Amoco's training initiative reduces wellsite drilling problems. *Pet. Eng. Int.* **1995**, *67*, 3029–3035.
2. Hopkins, C.J.; Leicksenring, R.A. Reducing the risk of stuck pipe in the Netherlands. In Proceedings of the IADC/SPE Drilling Conference, Amsterdam, The Netherlands, 28 February–2 March 1995; pp. 757–766. [[CrossRef](#)]
3. Tomren, P.H. Experiment study of cuttings transport in Directional Wells. *SPE Drill. Eng.* **1986**, *1*, 43–56. [[CrossRef](#)]
4. Duan, M.; Miska, S.Z.; Yu, M.; Takach, N.E.; Ahmed, R.M.; Zettner, C.M. Critical Conditions for Effective Sand-Sized Solids Transport in Horizontal and High-Angle Wells. *SPE Drill. Complet.* **2009**, *24*, 10. [[CrossRef](#)]
5. Li, J.; Wilde, G. Effect of Particle Density and Size on Solids Transport and Hole Cleaning with Coiled Tubing. In Proceedings of the SPE/ICoTA Coiled Tubing Conference and Exhibition, Woodlands, TX, USA, 12–13 April 2005; pp. 1–9. [[CrossRef](#)]
6. Ozbayoglu, M.E.; Osgouei, R.E.; Ozbayoglu, A.M. Hole Cleaning Performance of Gasified Drilling Fluids in Horizontal Well Sections. *CPS/SPE Int. Oil Gas* **2010**, *49*, 5–10. [[CrossRef](#)]
7. Han, S.M.; Woo, N.S.; Hwang, Y.K. Solid-liquid mixture flow through a slim hole annulus with rotating inner cylinder. *J. Mech. Sci. Technol.* **2009**, *23*, 569–577. [[CrossRef](#)]
8. Han, S.M.; Hwang, Y.K.; Woo, N.S.; Kim, Y.J. Solid-liquid hydrodynamics in a slim hole drilling annulus. *J. Pet. Sci. Eng.* **2010**, *70*, 308–319. [[CrossRef](#)]
9. Allahvirdizadeh, P.; Kuru, E.; Parlaktuna, M. Experimental investigation of solids transport in horizontal concentric annuli using water and drag reducing polymer-based fluids. *J. Nat. Gas Sci. Eng.* **2016**, *35*, 1070–1078. [[CrossRef](#)]
10. Ford, J.T.; Peden, J.M.; Oyenyin, M.B.; Gao, E.; Zarrough, R. Experimental Investigation of Drilled Cuttings Transport in Inclined Boreholes. In Proceedings of the 65th Annual Technical Conference and Exhibition of the Society of Petroleum Engineers, New Orleans, LA, USA, 23–26 September 1990; pp. 197–206. [[CrossRef](#)]

11. Hyun, C.; Shah, S.; Osisanya, S. A Three-Layer Modeling for Cuttings Transport with Coiled Tubing Horizontal Drilling. In Proceedings of the SPE Annual Technical Conference and Exhibition, Dallas, TX, USA, 1–4 October 2000; pp. 1–14. [[CrossRef](#)]
12. Kelessidis, V.C.; Bandelis, G.E. Flow Patterns and Minimum Suspension Velocity for Efficient Cuttings Transport in Horizontal and Deviated Wells in Coiled-Tubing Drilling. *SPE Drill. Complet.* **2004**, *19*, 213–227. [[CrossRef](#)]
13. Osgouei, R.E.; Ozbayoglu, M.E.; Fu, T.K. Cfd Simulation of Solids Carrying Capacity of a Newtonian Fluid through Horizontal Eccentric Annulus. In Proceedings of the ASME Proceedings | 13th International Symposium on Liquid-Solids Flows, Village, NV, USA, 7–11 July 2013; pp. 1–9. [[CrossRef](#)]
14. Larsen, T.I.; Pilehvari, A.A.; Azar, J.J. Development of a New Cuttings-Transport Model for High-Angle Wellbores Including Horizontal Wells. *SPE Drill. Complet.* **1997**, *12*, 129–135. [[CrossRef](#)]
15. Fokeer, S.; Lowndes, I.; Kingman, S. An experimental investigation of pneumatic swirl flow induced by a three lobed helical pipe. *Int. J. Heat Fluid Flow* **2009**, *30*, 369–379. [[CrossRef](#)]
16. Derksen, J.J. Simulations of confined turbulent vortex flow. *Comput. Fluids* **2005**, *34*, 301–318. [[CrossRef](#)]
17. Li, H.; Tomita, Y. Particle velocity and concentration characteristics in a horizontal dilute swirling flow pneumatic conveying. *Powder Technol.* **2000**, *107*, 144–152. [[CrossRef](#)]
18. Bali, T.; Sarac, B.A. Experimental investigation of decaying swirl flow through a circular pipe for binary combination of vortex generators. *Int. Commun. Heat Mass Transf.* **2014**, *53*, 174–179. [[CrossRef](#)]
19. Van Puymbroeck, L.; Williams, H.; Drilling, V.A.M. Increasing Drilling Performance in ERD Wells with New Generation Drill Pipe. In Proceedings of the Unconventional Resources Technology Conference, Denver, CO, USA, 12–14 August 2013; pp. 1060–1070.
20. Van Puymbroeck, L.; El Bachiri, K. New generation drill pipe to increase drilling performance in ERD wells. In Proceedings of the SPE/IADC Middle East Drilling Technology Conference & Exhibition, Dubai, UAE, 7–9 October 2013; pp. 7–9.
21. Ahmed, R.; Sagheer, M.; Takach, N.; Majidi, R.; Yu, M.; Miska, S.; Rohart, C.; Boulet, J. Experimental Studies on the Effect of Mechanical Cleaning Devices on Annular Cuttings Concentration and Applications for Optimizing ERD Systems. In Proceedings of the SPE Annual Technical Conference and Exhibition, Florence, Italy, 19–22 September 2010. [[CrossRef](#)]
22. Rodman, D.; Wong, T.; Chong, A.C. Steerable hole enlargement technology in complex 3d directional wells. In Proceedings of the SPE Asia Pacific Oil and Gas Conference and Exhibition, Jakarta, Indonesia, 9–11 September 2003.
23. Heitmann, N.; Chacinet, E.; Molero, R.; Graterol, W.; Servicios, P. Novel Integrated Hole-Cleaning Concept Reduces Well Construction By 3 Rig Days. In Proceedings of the IADC/SPE Asia Pacific Drilling Technology Conference, Bangkok, Thailand, 25–27 August 2014.
24. Fokeer, S.; Lowndes, I.S.; Hargreaves, D.M. Numerical modelling of swirl flow induced by a three-lobed helical pipe. *Chem. Eng. Process. Process Intensif.* **2010**, *49*, 536–546. [[CrossRef](#)]
25. Li, G.; Miles, N.J.; Wu, T.; Hall, P. Large eddy simulation and Reynolds-averaged Navier–Stokes based modelling of geometrically induced swirl flows applied for the better understanding of Clean-In-Place procedures. *Food Bioprod. Process.* **2017**, *104*, 77–93. [[CrossRef](#)]
26. Zhou, J.W.; Du, C.L.; Liu, S.Y.; Liu, Y. Comparison of three types of swirling generators in coarse particle pneumatic conveying using CFD-DEM simulation. *Powder Technol.* **2016**, *301*, 1309–1320. [[CrossRef](#)]
27. Syamlal, M.; O'Brien, T.J. *Computer Simulation of Bubbles in a Fluidized Bed*; Symposium Series 85; AIChE: Hoboken, NJ, USA, 1989; pp. 22–31.
28. Wen, C.; Yu, Y. Mechanics of Fluidization. *Chem. Eng. Prog. Symp. Ser.* **1966**, *62*, 100–111.
29. Gidaspow, D. *Multiphase Flow and Fluidization: Continuum and Kinetic Theory Descriptions*; Academic Press: Boston, MA, USA, 1994.
30. Pang, B.; Wang, S.; Liu, G.; Jiang, X.; Lu, H.; Li, Z. Numerical prediction of flow behavior of cuttings carried by Herschel-Bulkley fluids in horizontal well using kinetic theory of granular flow. *Powder Technol.* **2018**, *329*, 386–398. [[CrossRef](#)]
31. Pang, B.; Wang, S.; Wang, Q.; Yang, K.; Lu, H.; Hassan, M.; Jiang, X. Numerical prediction of cuttings transport behavior in well drilling using kinetic theory of granular flow. *J. Pet. Sci. Eng.* **2018**, *161*, 190–203. [[CrossRef](#)]
32. Ergun, S. Fluid flow through packed columns. *Chem. Eng. Prog.* **1992**, *48*, 89–94.

33. Huilin, L.; Gidaspow, D.; Bouillard, J.; Wentie, L. Hydrodynamic simulation of gas-solid flow in a riser using kinetic theory of granular flow. *Chem. Eng. J.* **2003**, *95*, 1–13. [[CrossRef](#)]
34. Shook, C.A.; Roco, M.C. *Slurry Flow: Principles and Practice*; Butterworth-Heinemann: London, UK, 1991.
35. Guédon, G.R.; Besagni, G.; Inzoli, F. Prediction of gas–liquid flow in an annular gap bubble column using a bi-dispersed Eulerian model. *Chem. Eng. Sci.* **2017**, *161*, 138–150. [[CrossRef](#)]
36. Beer, J.M.; Chigier, N.A. *Combustion Aerodynamics*; Applied Science Publishers LTD: London, UK, 1972.



© 2019 by the authors. Licensee MDPI, Basel, Switzerland. This article is an open access article distributed under the terms and conditions of the Creative Commons Attribution (CC BY) license (<http://creativecommons.org/licenses/by/4.0/>).